1K Element Antenna System for Mobile Direct Broadcasting Satellite Reception

Pedram Mousavi, *Member, IEEE*, Mohammad Fakharzadeh, *Member, IEEE*, and Safieddin Safavi-Naeini, *Member, IEEE*

***Abstract*—This paper describes the design methodology and low-cost solutions implemented in a low-cost 1K–element phased array system for mobile direct broadcasting satellite (DBS) reception. The techniques and configurations used to reduce the cost and complexity of the system are described in this paper. Moreover, the design of a novel compact sub-array antenna to reduce the overall size of the system , the signal processing unit to suppress the noise on feedback channel and the mechanical structure to make the system agile, light and low cost are presented. Three efficient, model-free beamforming techniques are discussed and their performances in terms of convergence speed and steady state behavior are compared using several road tests. Results show that the developed intelligent antenna can meet the stringent requirements of the highly dynamic mobile applications.**

***Index Terms*—Adaptive antenna, digital satellite broadcasting, mobile satellite communication, phased array antenna.**

I. Introduction

DEMANDS for mobile reception of high quality video and data broadcasting services are rapidly increasing. Satellite broadcasting has a unique advantage of wide area coverage as compared to terrestrial broadcasting. However, reliable, robust, low profile and low cost antenna system that can receive and maintain weak satellite signal for all road conditions and vehicle maneuvers are not commercially available.

Intelligent antennas can offer significant advantage in this field. Intelligent antennas refer to antenna system that adapts itself to users ever-changing requirements and the dynamic conditions of the environment by taking advantage of signal processing methods to adjust its radiation direction, frequency channel and polarization. They can reduce the size of the antenna which is an essential factor in market acceptability. Also by using electronic beamforming, the tracking speed substantially increases compared to the mechanical counterpart. The latter is important for compensating various road conditions and vehicle maneuvers. However, despite their impressive potentials and properties, intelligent antenna systems have not become widespread commercial products in this field. Cost and complexity of intelligent antennas are beyond the scales of consumer electronics devices [1]. Calibration is an essential requirement of such complex systems, which is a fairly time-consuming process and requires skilled manpower. Moreover, the narrow bandwidth of microwave components degrades the broadband performance of a phased array system. Finally, a majority of the beamforming algorithms developed so far either have preconditions, or require considerable hardware resources, which make them unsuitable for a low-cost phased array system [2]–[19].

To design a low-cost intelligent antenna system, several parameters, both at the component level and system level, must be noticed. At the component level, high gain antenna elements, low loss feed networks, low noise blocks, phase and amplitude linearity of active components and most importantly fabrication tolerances are among the factors that directly affect the cost. System integration and the issues arising from that have significant effects on the adaptability of the system to very cost sensitive applications such as vehicular communications. Some of those concerns are: mutual coupling, cross-talk between different channels, system linearity, signal isolation, resonance, element position error, element failure, weight, size, wind-loading and other mechanical constraints.

In [20] the authors have presented an intelligent antenna system for on-road DBS reception, operating at 12.2–12.7 GHz, with a novel electronic beamforming algorithm [21], which in conjunction with a mechanical stabilization loop provides a robust tracking algorithm to compensate for vehicle maneuvers [22]. This paper discusses novel features and new mechanism which are added to the system in four areas that significantly reduce the cost and complexity and advance the performance of the unit in highly hostile environments in terms of noise, interference, extreme temperatures, various weather conditions and sharp maneuvers. These areas are:

1) A novel sub-array antenna and power combiner/phase shifter box, which have direct effects on the radiation gain, total loss and size of the system.
2) The signal processing and detection modules, which reduce the noise and interference on the feed-back loop of the beamforming algorithm.
3) A light, agile and easily assembled mechanical platform with minimum vibration and noise transmission to the interior of the vehicles.
4) Three beamforming techniques, which are model-free (does not required the knowledge of phase-voltage, location of the target, and training sequence), converge fast,

Manuscript received July 30, 2009; revised March 22, 2010; accepted March 31, 2010. Date of publication June 10, 2010; date of current version August 20, 2010.

P. Mousavi is with Intelligent Mechatronics Systems Inc., Waterloo, ON N2J 2Z5, Canada (e-mail: Pedram.mousavi@gmail.com).

M. Fakharzadeh is with the Electrical and Computer Engineering Department, University of Waterloo, Waterloo, ON N2L 3G1, Canada, and also with the Intelwaves Technologies LTD, Waterloo, ON N2L 6J2, Canada.

S. Safavi-Naeini is with the Electrical and Computer Engineering Department, University of Waterloo, Waterloo, ON N2L 3G1, Canada.

Color versions of one or more of the figures in this paper are available online at http://ieeexplore.ieee.org.

Digital Object Identifier 10.1109/TBC.2010.2049611

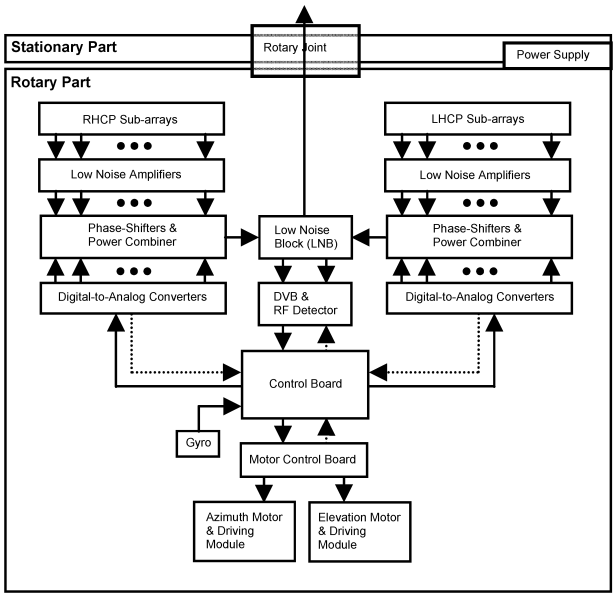

Fig. 1. Intelligent antenna system configuration for mobile DBS.

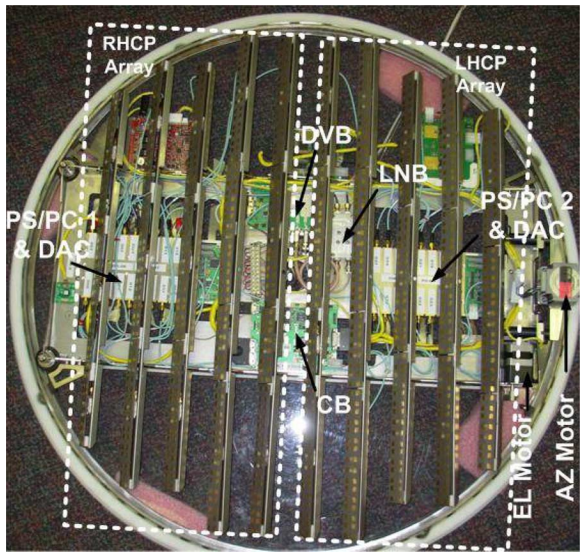

Fig. 2. Phased array antenna for land mobile satellite link (CB: control board; PS/PC: phase shifter power combiner; EL: elevation; AZ: azimuth).

and enable tracking the desired satellite on any driving condition and can compensate for the fabrication errors.

In the next section, we present the configuration of the intelligent antenna system. In Section III, the designed microwave components, including the new sub-array antenna and power combiner/ phase shifter will be described. Section IV is dealing with the agile low-profile mechanical structure of the antenna system. Section V elaborates on beamforming algorithms. The effectiveness of the proposed beamforming techniques is confirmed through various tests in Section VI. Finally, Section VII concludes the paper.

II. System Description

A. RF Section

Figs. 1 and 2 shows the system configuration and the photograph of the new version of the low-profile intelligent antenna system designed for vehicular satellite communication. Two operational modes have been designed for this system: Homing (acquisition of the desired satellite), and Tracking (maintaining the array beam locked on the satellite direction) [20]. The system consists of 17 high-gain sub-arrays for Right Hand Circular Polarization (RHCP) and 17 sub-arrays for Left Hand Circular Polarization (LHCP). Compared to the previous version [20], by introducing a novel design for the sub-array (see Section III-A) the overall gain has increased to 31.8 dBi from 31.5 dBi [20] and the axial ratio has decreased to 1.5 dB from 1.8 dB [20], while its size has decreased. As a result, the overall diameter and the height of system have reduced to 83 cm and 5 cm compared to 86 cm and 6 cm of [20], which make the new version more attractive for the consumer electronic market and easier to install on vehicles.

The sub-array antennas for each polarization are placed in five consecutive panels fitted in a half-circle. Three panels hold three sub-array antennas and the rest hold four sub-arrays. Each sub-array consists of 16 or 32 microstrip patch elements and a feed network. Totally, 992 patch elements are used in this system.

Each sub-array is connected to a voltage controlled analog phase shifter [23] via an LNA and low-loss cable. For each polarization the outputs of all 17 phase shifters are combined by a power combiner and then down converted to IF by a Low Noise Block (LNB) module. The control voltage of the phase shifters are adjusted by the beamforming algorithm.

Since phase shifting devices are used instead of true-time delay network, there is a possibility of beam squint at the edge of the frequency band when the antenna is scanning. Due to the small scan angle in azimuth ($\pm 2.8^\circ$) the beam-squint in azimuth is less than 0.05° from the beam direction related to the center frequency. However, for elevation scanning, due to the larger scan angle (20°–70°) the beam-squint can be up to 4° from the main beam at center frequency. To alleviate this problem, different RF cable lengths between panels (as shown in Fig. 2) are employed in the new version. The required coaxial cable length between each sub-array and the corresponding phase shifter is given by

$$L_i = L_{\min} + (n - i)\Delta L/\sqrt{\varepsilon_r} \tag{1}$$

where $n = 5$ is the number of panels for each polarization, L_{min} is the minimum cable length used in the system $(i = n)$, ε_r is the relative permittivity of the coaxial cable (2.1 in this case) and ΔL is the average distance between panels when the panels rotate in the elevation plane.

B. Signal Processing Unit

The block diagram of the signal processing unit is shown in Fig. 3(a). The down-converted signal from the LNB (IF signal) transfers to the Digital Video Broadcasting (DVB) board developed in house and shown in Fig. 3(b). The IF frequency ranges from 950 to 1450 MHz, and its power level varies between -20 to -35 dBm. The IF signal is divided into two parts using a compact Wilkinson power divider. One branch goes to the Digital Satellite Tuner (ZL10037) and the Satellite Demodulator (ZL10313). The satellite ID, extracted from the MPEG2 stream, is used to identify the desired satellite and expedite the

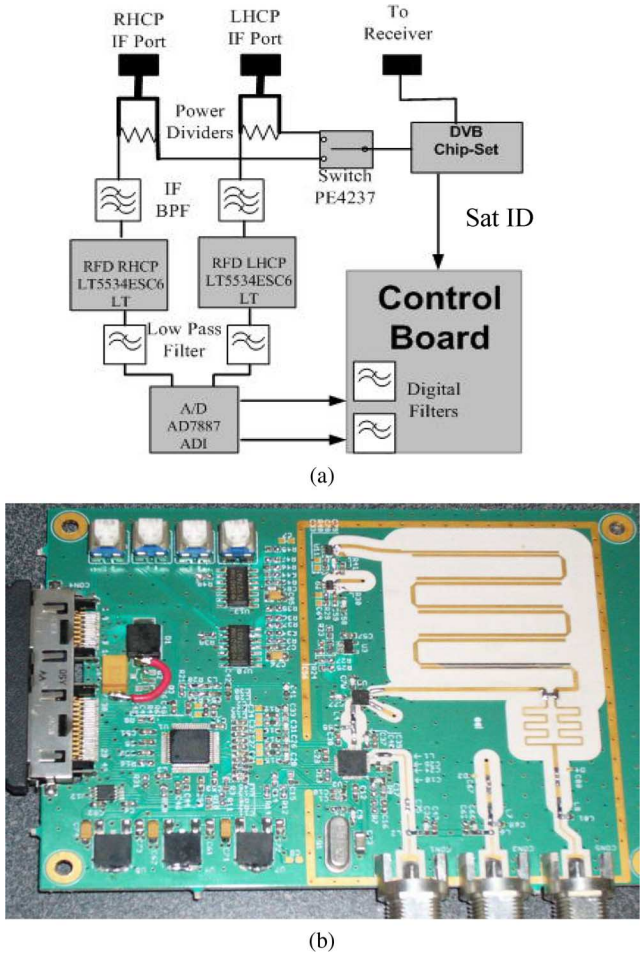

Fig. 3. (a) Block diagram of signal processing unit. (b) DVB and RF detector board.

initial homing of the phased array system. Also the amplified IF signal from the digital satellite tuner is transferred to the satellite receiver inside the car through a rotary joint. The other branch of the Wilkinson power divider is connected to the RF power detector via a band-pass hair pin filter. The power detector (LT5534) has a frequency range of 50 MHz to 3 GHz, and a dynamic range of 60 dB. The measured power is the only available input for the beamforming algorithms which will be discussed in Section V. The amplitude fluctuations of the measured power caused by noise or interference from other active sources can reduce the accuracy of the beamforming algorithm. Thus, three types of filters have been implemented in the signal processing unit to limit noise and interference.

A band-pass filter with 100 MHz bandwidth (1200–1300 MHz) is employed before the power detector. Additionally, a low-pass RC filter is implemented after the power detector to smooth the detected power level, which ideally must be a DC signal. The output is then digitized by a 12-bits analog to digital converter (AD7887) with a maximum symbol rate of 125 kS/s. Finally, a N-point low-pass digital filter with Hamming window and a cutoff frequency equal to 0.01 of the sampling rate is used after the ADC. Digital filtering attenuates the high-frequency components of the sampled measured power and limits the energy of noise. The size of Hamming window, N, can vary from 8 to 30. Increasing N diminishes the instantaneous power fluctuations, while decreasing N speeds up the beamforming.

The control algorithms, have been implemented in a Digital Signal Processor (ADSP-BF537) on the main Control Board (CB). Using the measured RF power level and the gyro information, the beamforming algorithm adjusts the phase shifters and the tracking algorithm sends the required commands to the azimuth and elevation motors, via motor control and motor driver boards.

III. RF and Microwave Components

In this section the design procedures for the new sub-array antenna and phase shifters–power combiner box are discussed and some measured data will be presented.

A. Sub-Array Antenna

The design criteria for the sub-array antenna are to achieve high radiation gain (>20 dBi), low feed-network loss, a good return loss (< -15 dB) and a small axial ratio (<2 dB) over a 4% relative bandwidth. Additionally, the width and the length of the sub-array must be reduced, which directly affect the overall height and diameter of the system.

In [20], 2×8 and 2×16 sub-arrays antenna were developed by arraying truncated-corner square patch antennas. Although satisfactory results in terms of gain, return loss and axial ratio were obtained, the mutual coupling between the elements prevented further size reduction without sacrificing gain and axial ratio. It is found that in the sequential rotation configuration the mutual coupling for circular polarized elements, increases rapidly by decreasing the distance between them. However, for the linear polarized element, this effect is less pronounced. Therefore, to maintain the gain and reduce the distance between the elements, the circular polarization of the patch needs to be perturbed up to some extend. In the new system, the optimization was performed on the patch shape, matching network and the applied phase between each two elements in a sequentially rotated 2×2 patch array. The optimization on the shapes of the patch antennas in a 2×2 configuration resulted in two notable irregular hexagonal microstrip (A &B) antennas as shown in Fig. 4. Due to the irregular shape of the patches, the new electrical phase shifts between the elements in sequential rotation are calculated to be 0°, 80°, 190°, and 270°. The simulated gain and axial ratio of each patch over three frequencies in the operating band are summarized in Table I. Simulation shows that the compact 2×2 sub-array using truncated corner patch has maximum gain of 11.86 dBi axial ratio varies between 0.3 to 1.3dB across the band. In comparison, the compact irregular 2×2 sub-array demonstrates 12.3 dBi gain and the axial ratio that varies between 0.2 and 0.7 dB.

The antenna substrate consists of a top and bottom layer of Rogers RT Duroid 5880 with dielectric constant of $\varepsilon_r = 2.2$ and the loss tangent of 0.0009 at 10 GHz. To achieve a larger bandwidth and a higher gain, the top substrate thickness is set to 1.57 mm (0.0625λ). The feed-network is constructed on the lower substrate with a thickness of 0.25 mm (0.01λ) to reduce radiation losses. Fig. 5 shows the new 2×16 sub-array and the previous one described in [20]. The overall width and length

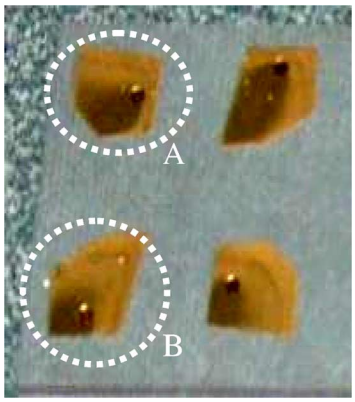

Fig. 4. Optimized patches, in a 2×2 sequentially rotated building block.

TABLE I
OPTIMIZED PATCH ANTENNA PARAMETERS

Antenna	Configuration 1 (Fig. 4, Patch A)			Configuration 2 (Fig. 4 Patch B)		
Frequency (GHz)	12.20	12.45	12.70	12.20	12.45	12.70
Return Loss (dB)	-15.7	-15.9	-14.3	-22.6	-27.5	-24.2
Gain (dBi)	6.59	6.63	6.68	6.36	6.44	6.51
Axial Ratio (dB)	2	1.39	3.14	1.53	1.85	2.78

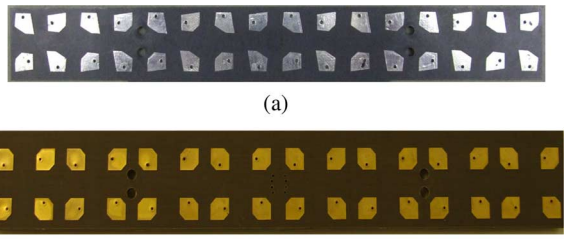

(a)

(b)

Fig. 5. Fabricated 2×16 sub-array antennas: (a) New sub-array; (b) Old sub-array [20].

of the new sub-array are 5 mm and 10 mm less than the previous sub-array shown in Fig. 5(b). Fig. 6 illustrates the measured radiation pattern in the principal azimuth and elevation planes of the sub-array at 12.5 GHz. The measured circular polarized gain is about 20.1 dBi. Considering a 0.5 dB loss added by the surface mount connector, the actual gain is estimated to be 20.6 dBi, which shows a 0.4 dB gain improvement over the gain of the sub-array antenna of Fig. 5(b). This can be attributed to the lower feed network loss and reduced mutual coupling. The measured axial ratio of the 2×16 sub-array is less than 1.35 dB across the band. The overall gain of the antenna system is 31.8 dBi and the axial ratio is less than 1.5 dB.

B. Power Combiner-Phase Shifter

Fig. 7 shows the 17 channel phase shifter–power combiner (PS/PC) box. In this system, the reflective-type phase shifters

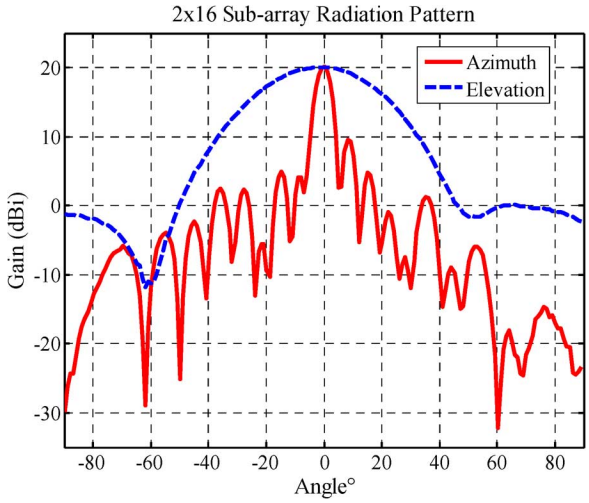

Fig. 6. Measured azimuths and elevation radiation patterns of the new 2×16 sub-array antenna shown in Fig. 5(a).

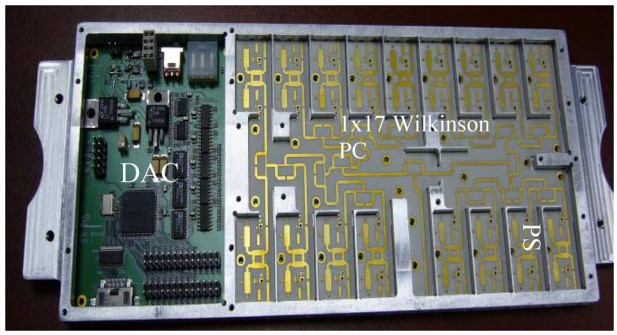

Fig. 7. Phase shifter power combiner box and DAC board.

(RTPS) are used [23], which consist of a 3 dB branch line coupler and low loss reflective loads connected to the through and coupled ports. The other ports of the coupler are symmetrically matched to 50 Ω. The 17 to 1 power combiner using a combination of two-way Wilkinson power combiners has been employed in this system.

The inside of the metallic enclosure is partitioned to minimize the undesirable coupling between ports. Also these partitions reduce the resonance inside the box significantly. Despite all these preclusions, in practice the PS/PC box resonates when certain combinations of voltages are applied to the phase shifters. To suppress the resonance, an absorber material was added to the lid of the PS/PC box.

The phase shifters are controlled by the voltages applied through the Digital to Analog Converter (DAC) board. The DAC board is assembled at the back of the PS/PC box to reduce the effect of DC and RF noise on control lines. The feeding lines for delivering power to the LNA are also supplied through the DAC board.

Fig. 8 shows the measured insertion loss (or gain) and phase shift versus the phase shifter control voltage of one channel for several frequencies ranging from 12–13GHz (8% relative bandwidth). Each channel includes a LNA (with 23–25 dB gain), a cable, a phase shifter and the power combiner. Fig. 8 indicates that the average amplitude gain varies from 1 to 3 dB and the phase shift is always more than 360° for a voltage range of 2

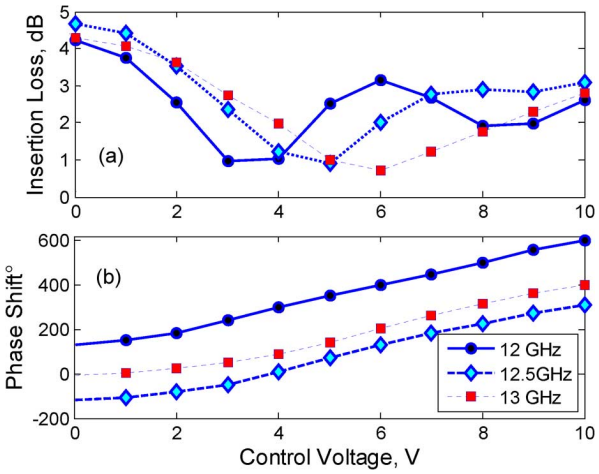

Fig. 8. Amplitude and phase variation over control voltages of one RF channel (including phase shifter, power combiner, cable and LNA).

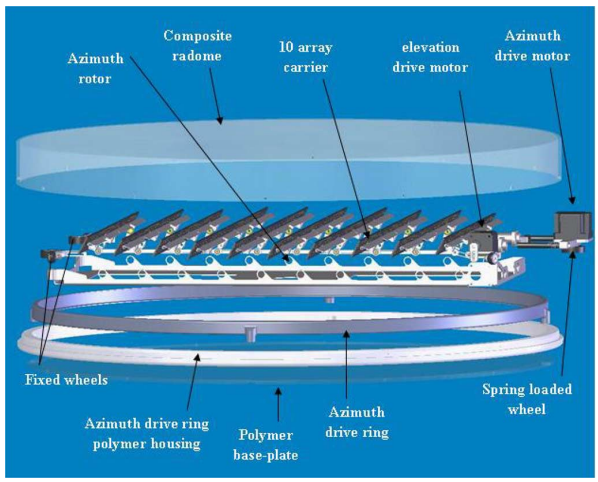

Fig. 9. An exploded isometric view showing the principal mechanical components of the low profile intelligent antenna system.

to 10 Volts. Therefore about 12 dB of ideal loss of the 17 to 1 power combiner is included in the measurements.

IV. Mechanical Structure

The general purpose of the mechanical design is to provide a light platform (less than 10 kg) for a low profile phased array satellite tracker system (5 cm height and 83 cm diameter), which can be fitted to small vehicles.

Fig. 9 shows a mechanical platform including a polymer base and a stainless steel azimuth rotation drive ring affixed to the inner diameter of the polymer base. An azimuth rotor assembly engages the rotation ring with two fixed wheels and one spring-biased urethane coated drive wheel of a stepper drive motor. One of the novel features of the mechanical structure is the spring loaded wheel which provides both optimized torque transmittal to the stainless steel drive ring, and, compensation for the thermal expansion of the different materials contained within the structure at various temperatures and environmental conditions. The other advantages of this structure are as follows:

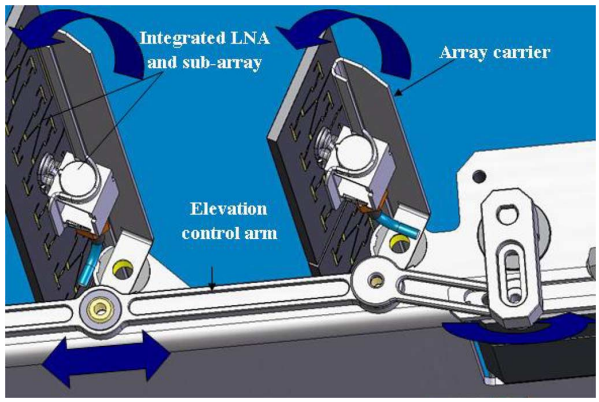

Fig. 10. A detailed view of elevation mechanism showing the elevation control arm and assembly of sub-array/LNA to array carrier.

1 By spring loading the drive assembly one can accurately provide torque which is sufficient to drive the rotor assembly without slippage, but not so high as cause unnecessarily high current demands on the entire drive system.
2 2) Spring loading compensates for the wide manufacturing tolerances required to produce the drive ring at an economical cost. The drive ring can actually be as much as $\pm 1/4''$ out of round or flatness and the system will still turn freely.

The urethane coating on all spring loaded and fixed wheels reduces noise and vibration. The unit is mechanically capable of rotating at speeds of up to $120^\circ/\mathrm{s}$, with acceleration values exceeding $100^\circ/\mathrm{s}^2$, within the drive ring/chassis structure. The elevation system enables the synchronous movement of ten antenna array panel assemblies by using the elevation control arms , shown in Fig. 10, from a position roughly 20° from the horizontal through to 90° i.e. a nominally 70° rotation.

By using the vertical transition between the LNA and the sub-array described in [20] it is possible to simply snap the integrated LNA and sub-array into the array carrier by hand, completely without any tools. This ability to position and attach 34 sub-array/LNA assemblies to array carriers drastically reduces the production cost. This new mechanical structure reduces the weight of the system by more than 30% compared to [22] (8 kg vs. 12 kg).

V. Efficient Beamforming Algorithm

In this section three beamforming algorithms designed for this phased array application are described. These algorithms do not depend on any specific initial conditions and the RF channel model. Their objective is to maximize the received power from the desired satellite whose ID has been detected by the DVB board and minimize the possibility and duration of loosing signal in various road and driving conditions.

A. Beamforming for Satellite Communication

There is a substantial body of research addressing the beamforming for phased array systems [24], [27]; however, efficient and low-complex algorithms are still needed to facilitate the utilization of phased arrays for commercial applications. An *efficient* beamforming algorithm is the one which compensates for the hardware inaccuracies, converges fast, reduces the steady

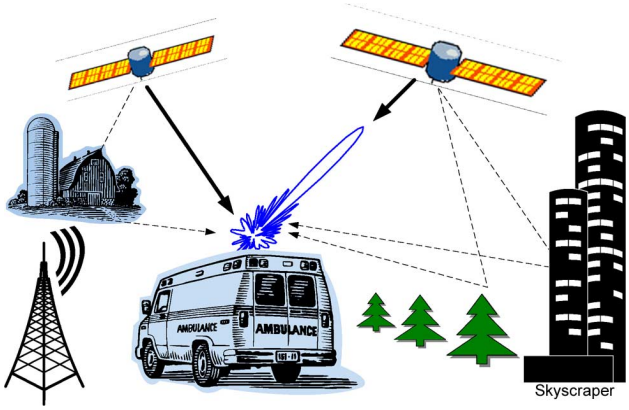

Fig. 11. A typical propagation environment for mobile satellite communication

state error, and does not add to the complexity of the system significantly.

Beamforming for geostationary satellite communication is not an interference-limited problem because, as shown in Fig. 11, the angular separation of the adjacent co-channel satellites (in azimuth plane) is much wider than the beamwidth of the high-gain antennas (2° for this system). Therefore, once the antenna is locked on the desired direction, the interference from the adjacent satellites is negligible.

B. Voltage Update Equation

For all proposed algorithms in this section, an iterative approach is used to update the control voltages of the analog Ku-band phase shifters. Let $\mathbf{v}(n) = [\mathrm{v}_1\ \mathrm{v}_2 \ldots \mathrm{v}_\mathrm{N}]$ denote the control voltage sequence of the N phase shifters at time n, which is the only variable of the beamforming problem. To update the control voltages and calculate $\mathbf{v}(n+1)$, first the approximate gradient of the received power with respect to the control voltages, denoted by $\hat{G}(n)$, is calculated. Next the voltages are updated according to [20]

$$v(n+1) = v(n) + 2\mu\hat{G}(n) \tag{2}$$

where μ is a positive scalar called *step size*. There are different methods to approximate the gradient of the power. One criterion to determine the proper method is the time-budget of the phased array system which gives the maximum convergence time of the beamforming process.

C. Convergence Time of the Beamforming Function

The developed phased array rotates in azimuth during its search mode and simultaneously performs the beamforming to find the satellite. Let T_S denote the time budget allocated to search the whole space. Then the minimum angular speed of the array is $\omega_{AZ} = 2\pi/T_S$. If $\Delta\theta_{AZ}$ denotes the beamwidth of the antenna in azimuth plane, then the maximum allocated time to search each azimuth step is given by

$$\Delta t = \frac{\Delta\theta_{AZ}}{\omega_{AZ}} \tag{3}$$

If N_{EL} directions in the elevation plane must be searched during Δt to find the desired satellite, then the convergence time of the beamforming algorithm ($\mathrm{t_{conv}}$) is limited by

$$t_{conv} \leq \frac{\Delta t}{N_{EL}} \tag{4}$$

There are two major sources of delay in any iterative beam-forming algorithm which uses the gradient estimation [25]. First, the time delay for updating the control voltages of the phase shifters and the internal delay in microwave circuits (t_{UP}). Second, the time delay to measure the RF power (reading ADC) and low pass filtering (t_{RF}). Both t_{UP} and t_{RF} are related to the analog to digital interface speed of the system. Let N_{UP} and N_{iter} respectively represent the number of independent power measurement required to calculate $\hat{G}(n)$ in (2), and the required number of beamforming iterations for convergence. The convergence time of the algorithm can be found from

$$t_{conv} = [N_{iter}N_{UP}(t_{UP} + t_{RF})] \tag{5}$$

Combining (3)–(5) we have

$$N_{iter}N_{UP} \leq \frac{\Delta\theta_{AZ}}{\omega_{AZ}N_{EL}(t_{UP} + t_{RF})} \tag{6}$$

All parameters on the right side of (6) are determined by the hardware constraints, while parameters on the left depend on the algorithm's performance. This inequality highlights the importance of designing an *efficient* beamforming algorithm to meet the time budget and other system design constrains.

D. Gradient Approximation Methods

Three methods have been applied in the new phased array system to estimate the gradient of the power. These methods are based on perturbing the control voltages of the phase shifters and measuring the received power after each perturbation.

1 Sequential One-Sided Approximation: The total received power is a function of the control voltages, $\mathbf{v}(n)$, so it can be denoted by $P[\mathbf{v}(n)] = P[\mathrm{v}_1(n), \ldots, \mathrm{v}_\mathrm{k}(n), \ldots, \mathrm{v}_\mathrm{N}(n)]$. In this method only one perturbation per phase shifter is applied to estimate each component of $\hat{G}(n) = [\hat{g}_1(n) \ldots \hat{g}_k(n) \ldots \hat{g}_N(n)]$,

$$\hat{g}_k(n) = \frac{P[v_1, \ldots v_k(n) \pm \delta, \ldots] - P[v_1, \ldots v_k(n), \ldots]}{\pm\delta} \tag{7}$$

where δ, called perturbation is an internal algorithm parameter. The beamforming algorithm which uses (7) is referred to as the *one-sided beamforming* algorithm. For this method $N_{UP} = N + 1$.

2 *Sequential Two-Sided Approximation:* In this method two sequential perturbations are applied to determine the centered finite-difference approximation of each gradient component,

$$\hat{g}_k(n) = \frac{P[v_1, \ldots v_k(n) + \delta, \ldots] - P[v_1, \ldots v_k(n) - \delta, \ldots]}{\delta} \tag{8}$$

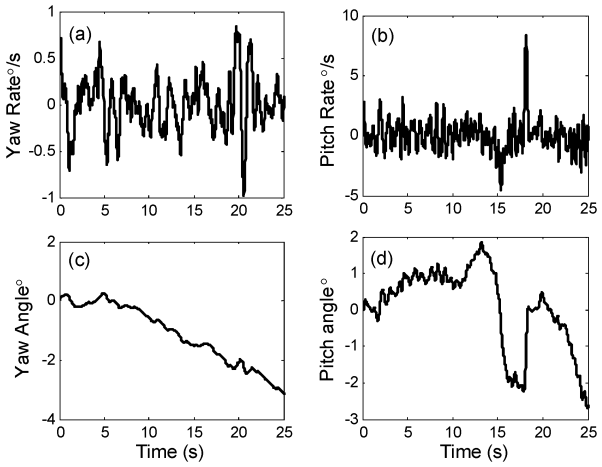

Fig. 12. Measured angular rates and calculated swept angles for the first test.

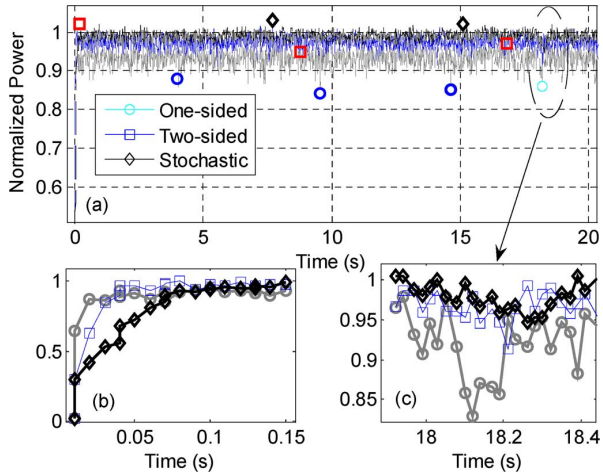

Fig. 13. Normalized power at the output of the phased array for the first road test.

The beamforming algorithm which uses (8) is referred to as the *two-sided beamforming* algorithm. For this method $N_{UP} = 2N + 1$. The criteria to select proper values for δ and μ have been discussed in [21], [26].

3 *Simultaneous Perturbation Approximation*: Despite to the previous methods, here all voltages are perturbed at the same time using a random perturbation vector $[\Delta_k]$. Two power measurements are used to estimate all components of $\hat{G}(n)$

$$\widehat{G}(n) = \frac{P([v_k] + [\Delta_k]) - P([v_k] - [\Delta_k])}{2}[\Delta_k]^{-1} \qquad (9)$$

This method is referred to as the *stochastic beamforming*. For this method N_{UP} is independent of the number of phase shifters and equals to 3 (2 updates to calculate (9) and 1 for (2)). So if the number of phase shifters increases, the speed of this method is not affected. A method for generating the random sequence $[\Delta_k]$ has been proposed in [25].

VI. Beamforming Results

Two road-tests were designed to evaluate the performance of the three beamforming methods presented in Section V. Rate sensors were installed on a van vehicle. The sampling rate of the gyro sensors was 100 Hz. For these tests, the processor was adjusted such that one iteration of the two-sided method was performed in 10 ms (half of the maximum speed). During this time almost two iterations of the one-sided technique and five cycles of the stochastic beamforming can be executed. The details of the servo-loop of this system have been described in [22].

A. First Road Test: Deceleration and Acceleration

The first road test consisted of 25s of deceleration and acceleration along a straight path. The bumps on the road and vehicle vibration cause small rotations around the pitch, yaw and roll axes. Fig. 12 shows the measured yaw (azimuth) and pitch rates and the calculated yaw and pitch angles. The yaw rate variation is limited to $\pm 1^\circ$ implying that the vehicle has moved on a straight path. There are two sharp peaks in the measured pitch-rate curve: one at 15.3 s and the other one at 18.2 s.

TABLE II
Statistical Analysis of Beamforming Techniques for the First Road Test

Beamforming Method	One-sided	Two-sided	Stochastic
Mean Received Power	93.4 %	99.0 %	98.9%
Standard deviation	2.65 %	1.05 %	1.55%

Fig. 13 compares the performance of the beamforming algorithms for this test. Table II summarizes the results, which shows the mean value of the normalized received power $\mu = \mathrm{E}[\mathrm{P_R}/\mathrm{P_{max}}]$ and standard deviation $\delta = \sqrt{E[(P_R/P_{\max} - \mu)^2]}$ for three beamforming techniques. For the 17-element phased array, the overall performances of the two-sided and stochastic methods are similar and better than the one-sided technique. However as Fig 13(b) illustrates the convergence of the one-sided technique is faster than the other two methods. Fig 13(c) shows a portion of the received power around 18.2s when the highest peak in Fig. 12(b) occurs. All curves descend at this point; however the performance of the two-sided method is slightly better than the other methods.

B. Second Road Test 360 Degree Turn

The second road-test includes a 360° turn. Fig. 14(a) shows the angular speed, which increases from $0^\circ/\mathrm{s}$ at $t = 3\,\mathrm{s}$ to $30^\circ/\mathrm{s}$ at $t = 5$ and hovers close to this value until $t = 15\,\mathrm{s}$. The fluctuations of pitch-rate are negligible compared to the yaw-rate variations. Fig. 15 and Table III compare the received power level for all three beamforming techniques. The two-sided technique is superior and outperforms the other methods. The received power by stochastic beamforming, as shown in Fig. 15(c), has several dips, because this technique needs more time to adapt itself to the fast variations. Fig. 15(b) shows that the one-sided method has the fastest convergence.

C. Fast Beamforming Technique

The maximum angular velocity of the vehicle during the 360° turn in Fig. 14 was limited to $30^\circ/\mathrm{s}$. Nevertheless as Fig. 15 indicates power fluctuation is a serious issue, for example, around $\mathrm{t} = 3.8\,\mathrm{s}$ the power level drops to below 50 % even for the two-sided beamforming technique. This situation is worsened if

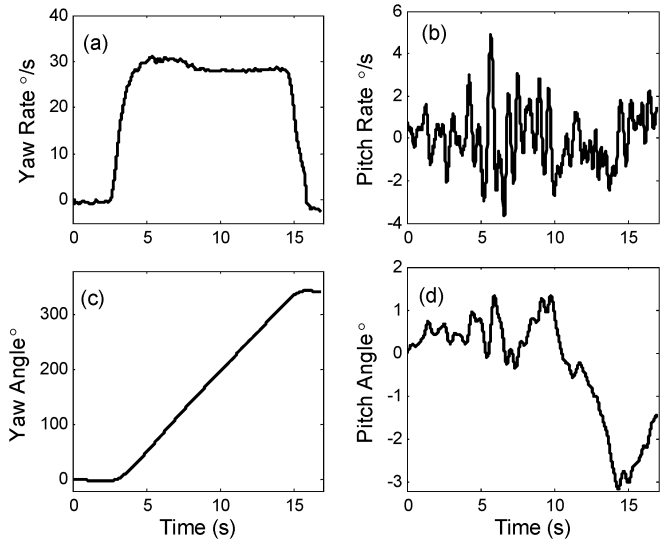

Fig. 14. Measured angular rates and calculated swept angles for the second road test.

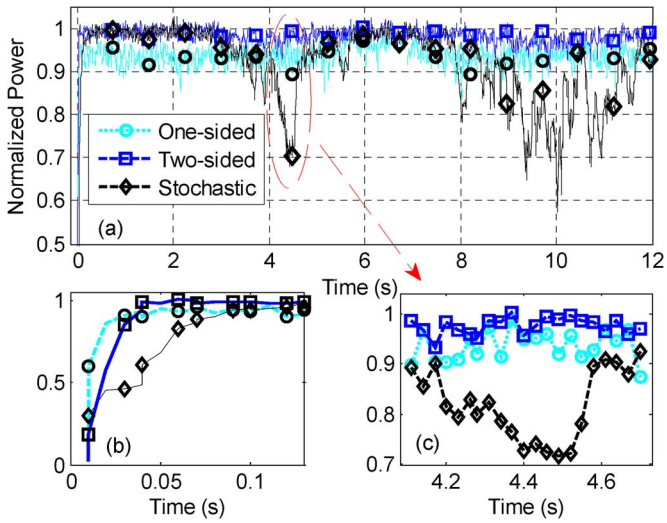

Fig. 15. Normalized power at the output of the phased array for the second test.

TABLE III
STATISTICAL ANALYSIS OF BEAMFORMING TECHNIQUES FOR THE SECOND ROAD TEST

Beamforming Method	One-sided	Two-sided	Stochastic
Mean Received Power	93.7 %	98.2 %	92.6%
Standard deviation	2.81%	1.80%	7.98%

the angular speed of the vehicle increases. A solution to restrict power outage, in other words increase the convergence speed, is to use an adaptive step-size (μ) in the voltage update equation (2) instead of a constant value. In [21] the authors have shown that the following equation for step size satisfies the fast convergence condition for a linear array

$$\mu_k = \left[\frac{\delta}{4\sin\delta}\frac{\sin\left(\gamma(n)/2\right)}{\sin\left(N\gamma(n)/2\right)}\right]\frac{\gamma(n)x_k/d}{\sin\left[\left(\frac{N+1}{2}-k\right)\gamma(n)\right]} \quad (10)$$

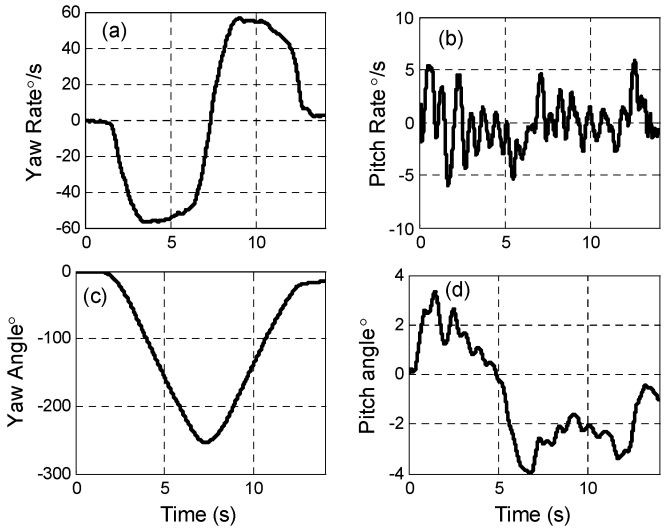

Fig. 16. Measured angular rates for the sharp S-turn manuever.

where d, x_k and N respectively denote the array spacing, position of the k-*th* antenna element (sub-array), and the total number of sub-arrays or phase shifters. Provided that the execution time of one iteration of the beamforming algorithm, ΔT, is adequately short, $\gamma(n)$ depends on the angular velocity and ΔT through the following relation [21]

$$\gamma(n) = k_o d\Delta T\dot{\theta}(n)\cos\theta(n-1) \quad (11)$$

Equation (10) combined with the two-sided gradient estimation in (8) is referred to as the *fast* beamforming technique in this work.

D. Beamforming for S-Shaped Turn Road Test

To verify the advantage of the fast beamforming method another road test was designed. This test consists of a sharp S-shaped maneuver of the vehicle shown in Fig. 16. In this test the angular velocity (yaw rate) varied from $-60°/\text{s}$ to $60°/\text{s}$. Each beamforming cycle (ΔT) was adjusted to 10 ms (half of the maximum beamforming speed). The adaptive step size for each antenna element/sub-array $(1 \le k \le 17)$ was calculated from

$$\mu_k(n) = (0.7 + 1.13|x_k|)\left[0.4 + 1.13|\dot{\phi}(n-1)|\right] \quad (12)$$

where x_k and $\dot{\phi}$ represent the x-coordinate of the element k relative to the array center in meter and the yaw rate of the vehicle in rad/s.

Fig. 17 compares the received power for the regular two-sided and fast beamforming techniques. It is seen that the depth and width of the fading dips have reduced significantly. For example, as Fig. 17(b) shows that the width of the fading region has decreased from 60 ms to 30 ms by fast beamforming.

To provide a fair comparison, two figures of merit are defined: $Cr_{0.9}$ and $Cr_{0.95}$, which represent the percentage of the received power samples which are below the 90% and 95% of the maximum power, respectively. Table IV compares $Cr_{0.9}$ and $Cr_{0.95}$ for the graphs shown in Fig. 17. It shows that the fast

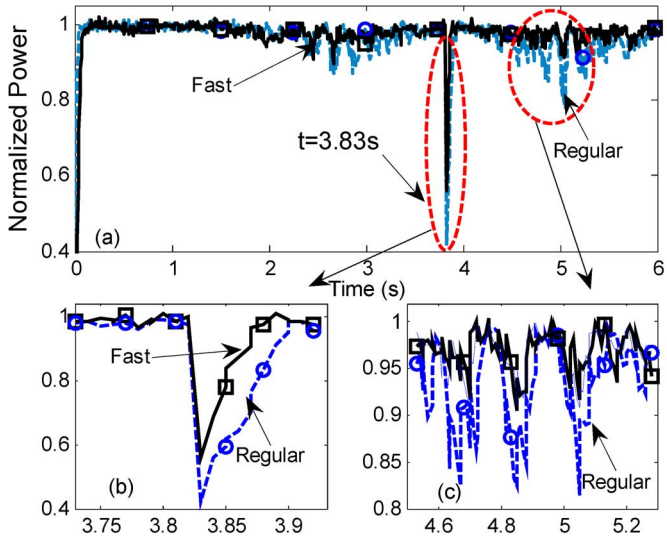

Fig. 17. Normalized power by fast beamforming and two-sided beamforming for the sharp S-turn maneuver.

TABLE IV
POWER FLUCTUATIONS OF FAST BEAMFORMING METHOD COMPARED TO THE TWO-SIDED BEAMFORMING TECHNIQUE

Beamforming Technique	$Cr_{0.9}$	$Cr_{0.95}$
Regular Two-sided	4.4%	17.5%
Fast Beamforming	0.75%	4.8%

beamforming technique is able to maintain the received power above the 90% level during the whole test.

E. Summary of the Beamforming Test Results

In summary, when the vehicle maneuver includes sharp turns the two-sided beamforming has a superior performance among all three methods. Using the fast convergence method and increasing the execution time of the algorithm reduce the probability of signal outage during fast maneuvers. For moderate maneuvers the stochastic method can be as efficient as the two-sided method for an array with 17 phase shifters. When the number of phase shifters/sub-arrays increases the stochastic method is promising to have a better performance. Moreover, the one-sided beamforming method has the fastest convergence, but the steady state error is not as low as that of the two-sided method.

F. Full Speed Operation of the System

In the previous tests the beamforming process was intentionally slowed to evaluate the performance of the different beamforming techniques. Fig. 18 shows the measured signal strength for a rapid S-turn test when the two-sided beamforming algorithm and the servo loop are operating at their full speed. Although the vehicle's angular acceleration exceeds $80^\circ/\mathrm{s}^2$, the azimuth angle error (pointing error) is limited to $\pm 1^\circ$ during the experiment. These results indicate that the developed intelligent antenna can meet the stringent requirements of highly dynamic on-road applications.

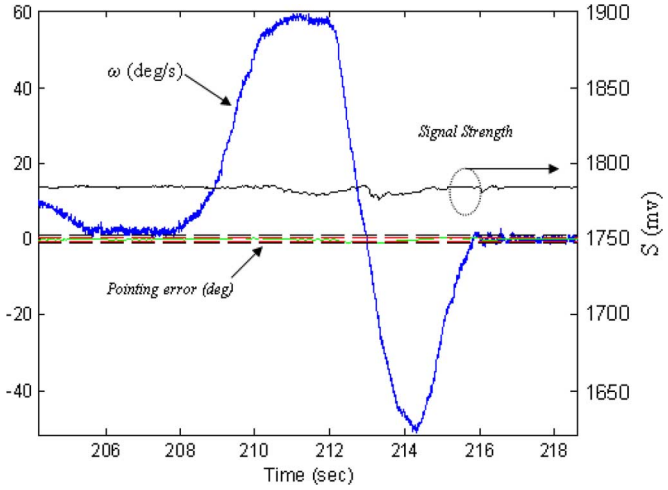

Fig. 18. Vehicle angular velocity (ω), pointing error and the satellite signal strength (35 mV is equal to 1 dBm).

VII. CONCLUSION

The novel aspects of the new version of an intelligent antenna system used for mobile satellite reception were discussed. These aspects include a novel compact sub-array, a signal processing unit, a phase shifter–power combiner box and a mechanical platform. The design methodology addressed techniques that reduce the cost, size and power consumption of mobile intelligent antennas. Three different beamforming algorithms were elaborated and compared with each other for various vehicle maneuvers. It was shown that the two-sided beamforming along with variable step size incorporated in fast beamforming technique is able to maintain the received power level above the 90% in any road test circumstances. The beamforming algorithms used in this paper were model-free, and can compensate for the inaccuracy associated with parts of the hardware. This paper demonstrated by meticulously designing components, system architecture and algorithm, one can adapt intelligent antennas to very cost sensitive applications such as vehicular communications.

ACKNOWLEDGMENT

The authors would like to thank Intelwaves Technologies LTD, Ontario Centers of Excellence (OCE), National Science and Engineering Research Council of Canada (NSERC), and Research In Motion (RIM) for their financial supports.

REFERENCES

[1] P. Mousavi, M. Fakharzadeh, and S. Safavi-Naeini, "A low-cost 1K element phased array antenna," in *IEEE Int. Microw. Symp. (IMS 2009)*, Boston, MA, USA, Jun. 7–12, 2009.

[2] T. Ohira, "Adaptive array antenna beamforming architectures as viewed by a microwave circuit designer," in *Asia-Pacific Microw. Conf.*, Dec. 3–6., 2000, pp. 828–833.

[3] N. Khandelwal and R. W. Jackson, "Active antenna module for low cost electronically scanned phased arrays," *IEEE Trans. Microw. Theory Tech.*, vol. 56, no. 10, pp. 2286–2292, Oct. 2008.

[4] L. Shafai, S. K. Sharma, M. Daneshmand, and P. Mousavi, "Phase shift bandwidth and scan range in microstrip arrays by the element frequency tuning," *IEEE Trans. Antenna Propag.*, vol. 54, no. 5, pp. 1467–1473, May 2006.

[5] J. Litva *et al., Digital Beamforming in Wireless Communications.*. Boston, London: Artech House, 1996, ~~28-34.
[6] F. Kira *et al.*, "New design approach to multiple-beam forming network for beam-steerable phased array antennas," *IEICE Trans. Electron., E82-C*, vol. 7, p. 11951201, Jul. 1999.
[7] A. D. Monk and C. O. Adler, "Calibration and RF test of Connexion by Boeing airborne phased arrays," in *IEEE Int. Symp. Phased Array Syst. Technol.*, Oct. 14–17, 2003, pp. 405–410.
[8] A. Agrawal and A. Jablon, "A calibration technique for active phased array antennas," in *IEEE Int. Symp. Phased Array Syst. Technol.*, Oct. 14–17, 2003, pp. 223–228.
[9] R. Sorace, "Phased array calibration," *IEEE Trans. Antennas Propag.*, vol. 49, no. 4, pp. 517–525, Apr. 2001.
[10] D. Goshi, K. Leong, B. Houshmand, and T. Itoh, "A Sparse Ka-band digital beamforming integrated receiver array," in *IEEE MTT-S Int. Microw. Symp. Digest*, Jun. 11–16, 2006, pp. 461–464.
[11] D. D. Curtis, C. R. Thomas, and W. J. Payne, "32-channel X-band digital beamforming plug-and-play receive array," in *IEEE Int. Symp. Phased Array Syst. Tech.*, Oct. 14–17, 2003, pp. 205–210.
[12] L. Kuehnke, J. Heminger, F. Klefenz, and A. Dreher, "A prototype digital beamforming antenna for future satellite communications," in *29th Eur. Microw. Conf.*, Munich, 1999, pp. 141–144.
[13] A. Dreher, N. Niklasch, F. Klefenz, and A. Schroth, "Antenna and receiver system with digital beamforming for satellite navigation and communication," *IEEE Trans. Microw. Theory Tech.*, vol. 51, no. 7, pp. 1815–1821, Jul. 2003.
[14] W. Li, X. Huang, and H. Leung, "Performance evaluation of digital beamforming strategies for satellite communications," *IEEE Trans. Aerosp. Electron. Syst.*, vol. 40, no. 1, pp. 12–26, Jan. 2004.
[15] J. D. Fredrick, Y. Wang, S. Jeon, and T. Itoh, "A smart antenna receiver array using a single RF channel and digital beamforming," in *IEEE MTT-S Int. Microw. Symp. Digest*, Jun. 11–16, 2002, pp. 313–316.
[16] D. S. Goshi, Y. Wang, and T. Itoh, "A compact digital beamforming SMILE array for mobile communications," *IEEE Trans. Microw. Theory Tech.*, vol. 52, no. 12, pp. 2732–2738, Dec. 2004.
[17] D. Spendley, L. J. Rosal, and D. D. Curtis, "Initial demonstration of and X-band digital beamforming (DBF) receive array," in *IEEE Aerosp. Conf. 2006*, pp. 1–10.
[18] S. Jeon, Y. Kim, and D. Oh, "A new active phased array antenna for mobile direct broadcasting satellite reception," *IEEE Trans. Broadcast.*, vol. 46, no. 1, pp. 34–40, Mar. 2000.
[19] Y. Ito and S. Yamazaki, "A mobile 12 GHz DBS television receiving system," *IEEE Trans. Broadcast.*, vol. 35, no. 1, pp. 56–62, Mar. 1989.
[20] P. Mousavi, M. Fakharzadeh, S. H. Jamali, K. Narimani, M. Hossu, H. Bolandhemmat, G. Rafi, and S. Safavi-Naeini, "A low-cost ultra low profile phased array system for mobile satellite reception using zero-knowledge beamforming algorithm," *IEEE Trans. Antennas Propag.*, vol. 56, no. 12, pp. 3667–3679, Dec. 2008.
[21] M. Fakharzadeh, S. H. Jamali, P. Mousavi, and S. Safavi-Naeini, "Fast beamforming for mobile satellite receiver phased arrays: theory and experiment," *IEEE Trans. Antennas Propag.*, vol. 57, no. 6, pp. 1645–1654, Jun. 2009.
[22] H. Bolandhemmat, M. Fakharzadeh, P. Mousavi, H. Jamali, Gh. Rafi, and S. Safavi- Naeini, "Active stabilization of a vehicle-mounted phased array antenna system," *IEEE Trans. on Veh. Technol.*, vol. 58, no. 6, pp. 2638–2650, Jul. 2009.
[23] P. Mousavi, I. Ehtezazi, S. Safavi-Naeini, and M. Kahrizi, "A new low cost phase shifter for land mobile satellite transceiver," in *Proc. IEEE Int. Symp. Antennas Propag.*, Jul. 2005, pp. 229–232.
[24] M. Fakharzadeh, "Optical and microwave beamforming for phased array antennas," Ph.D. dissertation, University of Waterloo, Waterloo, ON, Canada, Nov. 2008.
[25] M. Fakharzadeh, H. Jamali, S. Safavi-Naeini, P. Mousavi, and K. Narimani, "Fast stochastic beamforming for mobile phased array antennas," in *Proc. 2007 IEEE Int. Symp. Antennas Propag.*, Honolulu, Hawaii, USA, pp. 1945–1948.
[26] M. Fakharzadeh, S. H. Jamali, K. Narimani, P. Mousavi, and S. Safavi-Naeini, "Zero-knowledge beamforming for mobile satellite phased array antenna," in *68th IEEE Veh. Technol. Conf. (VTC 2008)*, Calgary, AB, Canada.
[27] R. J. Mailloux, *Phased Array Antenna Handbook*. Norwood, MA: Artech House, 1994.

Pedram Mousavi (S'96-M'01) received the B.Sc. (Hons.) degree in telecommunication engineering from Iran University of Science and Technology, Tehran, Iran, in 1995 and the M.Sc. and Ph.D. degrees in electrical engineering from the University of Manitoba, Winnipeg, MB, Canada, in 1997 and 2001 respectively.

From 2001 TO 2003, he was a Senior Microwave Engineer with Sirific Wireless Corporation, where he worked on the development of multiband VCO for various wireless standards. From 2003 to 2004, he was a Postdoctoral Fellow with the Department of ECE and the Centre for Integrated RF Engineering, University of Waterloo, Waterloo, ON, Canada, where he conducted research on low-cost low-profile phased array antenna system for mobile satellite communication. Based on his research with the University of Waterloo, he founded Intelwaves Technologies, wherein he was the CEO for four years. He is currently a Senior Research Scientist with Intelligent Mechatronics Systems Inc., Waterloo. His research interest includes miniaturized intelligent antennas and radios, microwave and millimeter-wave low-profile/integrated adaptive antenna structures, and emerging technologies for microwave and millimeter wave in smart antennas.

Mohammad Fakharzadeh (S'05-M'09) received the B.Sc. degree (honors) in electrical engineering from Shiraz University, Shiraz, Iran, in 2000 and the M.Sc. degree in electrical engineering from Sharif University of Technology, Tehran, Iran, and 2002.

From 2004 to 2008, he was a Ph.D. student with the Intelligent Integrated Radio and Photonics Group, University of Waterloo, Waterloo, ON, Canada, where he is currently a Postdoctoral Researcher and the Coordinator of the Millimeter-Wave Group. From January 2003 to September 2004, he was a faculty member with the Electrical Engineering Department, Shahid Chamran University of Ahvaz, Ahvaz, Iran. Since June 2005, he has been a Consultant with the Intelwaves Technologies Ltd., Waterloo, ON, Canada, where he has been developing the beamforming, signal processing, and tracking algorithms for Ku-band mobile satellite receiver-phased array antennas. His areas of interest include phased array design and beamforming, integrated antennas, millimeter-wave systems for short-range wireless networks, and miniaturized optical delay lines.

Dr. Fakharzadeh was the recipient of the University of Waterloo Outstanding Graduate Studies Award and the 2008 Khwarizimi International Award.

Safieddin Safavi-Naeini (M'79) was born in Gachsaran, Iran, in 1951. He received the B.Sc. degree in electrical engineering from the University of Tehran, Tehran, Iran, in 1974 and the M.Sc. and Ph.D. degrees in electrical engineering from the University of Illinois at Urbana-Champaign, in 1975 and 1979, respectively.

He was previously with the Electrical Engineering Department, University of Tehran, where he was an Assistant Professor in 1980 and an Associate Professor in 1988. Since 2002, he has bee a Full Professor with the Electrical and Computer Engineering Department, University of Waterloo, Waterloo, ON, Canada. He has been a scientific and technical consultant to a number of national and international telecommunication industrial and research organizations since 1980. His research interests and activities include numerical electromagnetics applied to RF/microwave/millimeter wave systems and circuits, antenna and propagation, wireless communication systems, very high speed digital circuits, and optical communication systems.